Marine Doppler Radar Surface Current Measurements in the Surf Zone

Dragana Perkovic
and Stephen J. Frasier
Microwave Remote Sensing Laboratory
Electrical and Computer Engineering
University of Massachusetts
Amherst, MA 01003
Email: perkovic@mirsl.ecs.umass.edu

Thomas C. Lippmann
Byrd Polar Research Center
Department of Civil and Environmental Engineering
Ohio State University
Columbus, OH 43210
Email: lippmann.2@osu.edu

***Abstract*—This paper presents a comparison of microwave radar surface velocity estimates to the estimates derived from video observations in the surf zone. The data presented here were collected during the Nearshore Canyon Experiment (NCEX) in the fall of 2003. The radar estimates are inferred from the Doppler shift of the backscattered radiation while video velocity estimates were produced using Particle Image Velocimetry (PIV) technique. Comparisons of longshore velocity estimates show high spatial correlation within the central surf zone. The comparisons of the near cross-shore velocity shows the importance of bore velocity removal while showing high spatial correlation when the bias is removed. Both alongshore and cross-shore velocity estimates display discrepancies in the breaker and the swash zones.**

I. Introduction

Much of the field research in the nearshore zone has been accomplished with *in-situ* measurement techniques using instruments such as pressure sensors and current meters fixed on pipes jetted into the sandy bottom [1], or from instruments mounted on moving platforms such as drifters e.g. [2]. However the nearshore is difficult to study comprehensively using only *in-situ* instrumentation because, for example, a substantial number of instruments are required to adequately sample the scales associated with nearshore circulation, typically on the order of $10^3 - 10^4$ m, the instruments present a hazard to recreational swimmers, surfers or boaters, and are difficult to install and maintain in the harsh nearshore environment for a given length of time. Recently remote sensing technology has been applied to studies of nearshore processes. Remote sensors are less invasive, are generally easier to deploy and maintain, and offer wider areal coverage than typical arrays of *in-situ* instruments. However, because the remote measurements are indirectly related to the quantity of interest, field verification is required to establish the validity of the measurements and to understand their limitations.

Use of video imagery to detect surface currents relies on adequate contrast of features on the surface which can be tracked. This usually requires adequate lighting conditions, which generally limits its utility to daylight hours and to regions within or just beyond the surf zone where foam and bubbles generated by the breaking process create contrast with the ambient water and provide a means to observe currents by quantifying the passive advection of features.

Radar, on the other hand, is generally insensitive to visibility conditions in the atmosphere and thus offers the possibility of making observations continuously over large spatial areas. It also offers a "direct" measurement of surface velocity (through the Doppler effect). Although spatial resolution of radar imagery is generally inferior to that of optical techniques, it has potential to generate useful data in conditions where video data are generally unavailable.

This paper describes observations of the surf zone currents and current fields made by radars during NCEX. Findings are compared to observations from video data. They prove to carry the same information and this encourages future extensive use of radar in nearshore ocean remote sensing. This validation should enable scientists to use radar data products in conjunction with video and/or when video data are not available at low visibility conditions. Section II describes remote sensing techniques used in the nearshore zone focusing on scattering of the electromagnetic radiation from the ocean surface and particle image velocimetry. Section III details the hardware used and the field experiment. Section IV describes the comparisons between radar and video observations of the surfzone. Observation of longshore and near cross-shore surface currents in the low wind conditions have been shown to be collocated in radar and video images and show good correlation leading us to believe that surface current flows in the nearshore can be correctly imaged by both remote sensing techniques under conditions of low wind. Section V offers explanations of differences observed in the comparison. Section VI summarizes the results and suggest possible future developments in this area of remote sensing.

II. Review of the remote sensing techniques in the nearshore zone

A. Microwave remote sensing of the ocean surface and Bragg scattering

A radar receives a signal with power P_r given by the radar equation

$$P_r = \frac{P_t G^2 \lambda^2 \sigma^0 \mathrm{d}A}{(4\pi)^3 R^4} \tag{1}$$

where P_t is the peak power transmitted by the radar, G is the antenna gain, σ^0 is the normalized radar cross-section (NRCS) of the surface observed, $\mathrm{d}A$ is the illuminated area, and R is the range to the target. The NRCS depends on physical properties of the target and the dominant scattering mechanism [3].

For moderate incidence angles (between 20° and 70°) Bragg/composite surface scattering has been shown to explain most of the features of the sea surface backscatter. Bragg scattering requires the surface to be "slightly rough", meaning surface displacement is small compared to the vertical component of the probing electromagnetic wavenumber. It neglects multiple scattering and assumes incident radiation illuminates the entire surface [4].

The composite surface theory does not, however, fully explain scattering within the surf zone, where the surface is often covered by foam from breaking waves and where the condition of slightly rough surface is often violated. Radar backscatter is significant in the surf zone even in low wind conditions [5] since most of the roughness is mechanically generated rather than wind generated. Figure 1(a) shows a 9-minute time-averaged image of radar backscatter. Bright areas indicate regions of strong backscatter while dark areas indicate regions of low backscatter. The Doppler effect is the change in the frequency and the wavelength of a received electromagnetic wave resulting from the relative velocity between the source of the electromagnetic radiation and the target. The change in frequency due to the motion of the observed target is given by$\Delta f = 2vf/c$ where f is the transmitted frequency of the electromagnetic radiation, c is the speed of light, and v is the relative velocity between the source and the target.

The mean Doppler shift is calculated from radar data by means of a very efficient covariance estimator or "pulse pair" technique. The pulse pair calculation estimates the first moment of the Doppler spectrum using the phase difference of echoes from successive pulses [6]. The velocity estimate is given by

$$v(t) = -\frac{\lambda}{2\pi} \frac{\phi(t)}{2\tau \sin\theta_i} \tag{2}$$

where λ is the radar wavelength, θ_i is the local angle of incidence between the incident radar pulse and the ocean surface, and $\phi(t)$ is the angle of covariance of successive pulses,

$$\phi(t) = \angle(\langle E_i E_{i-1}^* \rangle) \tag{3}$$

This phase difference is proportional to the displacement of a scatterer over the time period of τ seconds.

The apparent radial velocity determined from Doppler centroid includes several contributions. These include the phase velocity of Bragg resonant capillary waves (assuming Bragg scattering dominates), the line-of-sight component of the surface current including tidal currents, and the line-of-sight component of orbital velocity of larger scale surface waves [7], [8]. Hence, to extract a true surface current measurement from a Doppler velocity measurement the contributions of Bragg-scattering and orbital velocities of waves should be removed. The first component in many cases is considered constant on the time scale of several seconds so that the temporal variation in the Doppler velocity is dominated by the wave orbital velocity. This has been exploited as a means to characterize the so-called radar Modulation Transfer Function (MTF) relating the radar echo power to surface wave slope [3].

B. Video remote sensing technique

The contrast in video images comes from changes in brightness due to wave breaking and from reflection of incident light off the sea surface. The sharp contrast between specular scattering of light from foam and bubbles generated by breaking waves and bores and non-breaking (darker) water provides the primary signal used to infer nearshore processes. For example, time averaging video images over several minutes, produces a smooth pattern of average wave breaking distribution qualitatively related to patterns of wave dissipation [9], [10]. Figure 1(b) shows a video intensity composite image. The time-averaged imagery from each camera view is extracted separately over the same time period then overlaid on top of one another to produce a mosaic. The bright area in the image is produced by wave breaking in the surf zone. The darker areas are regions where there is no significant breaking. Only the highly dynamic region of the surf zone produces the necessary contrast to detect surface currents.

Particle Image Velocimetry is a technique where an identified tracer or a textural pattern is optically tracked with video over time producing velocity components associated with their movement. The main assumption of the PIV method is that the particles are passively advected by the flow. In the nearshore foam on the surface serves as the tracer. An area of interest is selected within a pair of rectified (ortho-normal) video images, for example, a region corresponding to the surf zone and extending down the coast a given distance dependent on the image resolution. Then a square search window, I, is selected from the first image and correlated with many spatially lagged search windows with the same dimensions, S, obtained from the second image separated by a small time Δt. PIV then relies on results of comparisons made by the Motion Estimation Processor (MEP) given by,

$$\Phi_{i,j} = 1 - \frac{\sum_1^a \sum_1^b (|I - S|)}{2 \sum_1^a \sum_1^b (I)} \tag{4}$$

where i and j are spatial indicies and a and b are pixel dimensions of I.

A 2D Gaussian distribution is fit to the peak of MEP matrix to estimate displacements (Δx, Δy) with sub-pixel resolution,

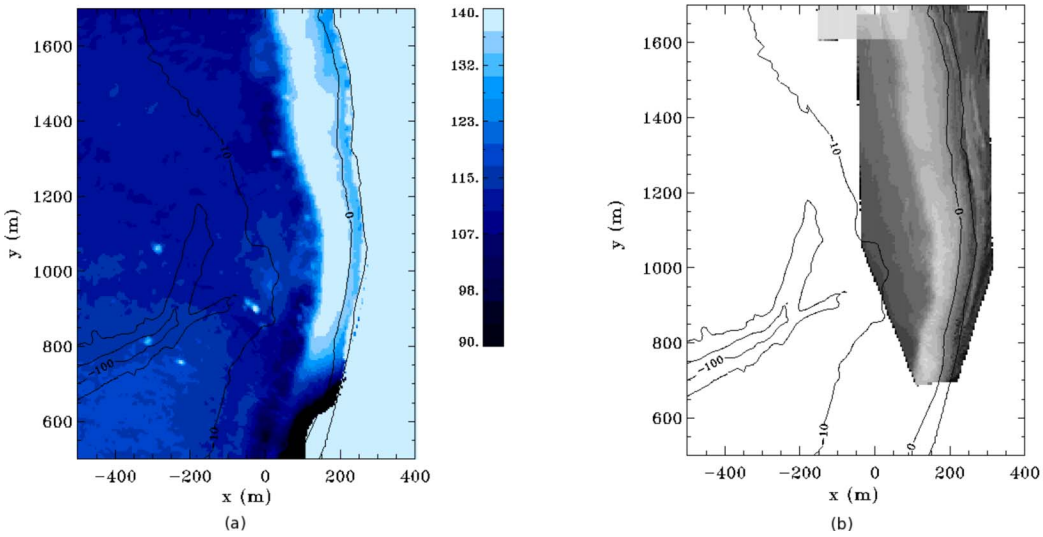

Fig. 1. Images of data collected on October 31st 2003 at 10am PST in La Jolla, Ca during NCEX experiment (a) UMass radar averaged backscattered power (b) Merged video intensity image from Ohio State video cameras.

[11]. Cross-shore and along-shore velocity magnitudes are calculated as u and v respectively,

$$u = \frac{\Delta x}{\Delta t}, v = \frac{\Delta y}{\Delta t} \tag{5}$$

Instantaneous velocities obtained with PIV are inherently noisy and must be filtered to remove spurious vectors. Typically velocity vectors are compared with neighboring vectors and then replaced if they exceed a threshold in either magnitude or direction [11], [12], [13]. Video derived PIV velocities used in this paper were smoothed with scales $2 \times I$ using optimal interpolation [14].

III. Field Experiment and Instrumentation

A. Nearshore Canyon Experiment (NCEX)

The Nearshore Canyon Experiment (NCEX) was conducted over two months, October and November of 2003 in La Jolla, California. NCEX was aimed at understanding the influence of complex offshore bathymetry, such as that of the La Jolla and Scripps submarine canyons, on wave transformation, nearshore circulation and the evolution of nearshore bathymetry [15]. Several research groups participated in this experiment both with in-situ instruments as well as remote sensing equipment.

The Microwave Remote Sensing Laboratory at UMass deployed two specially modified marine radars, at two locations along the coast in La Jolla, [16]. Figure 2(a) shows one of them deployed on the roof of the NOAA Southwest Fisheries Science Center (SWFSC) building. Radar data were processed in real-time to produce relative backscatter power, mean Doppler velocity and coherence. Both radars overlooked the area of the ocean above the Scripps canyon and instruments of the other research groups. The video cameras deployed in the NCEX experiment could retrieve data only during the daytime hours and in good visibility which is a limitation of video remote sensing technique. Video data used in this paper were collected by Ohio State University and from here on the video data will refer only to OSU data. Besides remote sensing instrument deployment during NCEX, a multitude of in-situ current meters and pressure sensors were deployed along the coast in line with cross shore transects.

The two radars deployed by UMass were the only microwave remote sensors deployed during NCEX providing a unique data set that recorded data simultaneously with the in-situ and optical remote sensors. The availability of various types of data relying on different physical phenomena to sense the nearshore processes will enable scientist to extract and compare observations gaining additional insight into nearshore zone.

B. Hardware description

1) Radars: The radars used to collect the data during NCEX were two identically modified Raytheon ST/MK2 high-seas marine navigation radars.

The original Raytheon ST/MK2 radar included: antenna, pedestal, transceiver unit and a video display, providing the magnitude of the received echoes as its output. The modifications to the original Raytheon ST/MK2 system include: (1) change of antenna polarization, (2) addition and replacement of some RF components (detailed later) in the existing RF unit, and (3) addition of host PC with data acquisition and counter/timer cards. These modifications were made to enable recording of the transmitted pulse into the data stream, therefore enabling Doppler pulse pair processing.

Ocean surface echo is stronger at vertical polarization [17], thus the antenna's polarization was changed to vertical by the addition of a meander-line polarizing grid on the radome covering the slotted array. The high power electromagnetic source used in both the original and the modified system is a magnetron. It is capable of producing a peak power of 25 kW. The magnetron by its nature has a random phase from pulse

(a) (b)

Fig. 2. Instrument deployment during NCEX on the roof of the SWFSC building in La Jolla, Ca. (a) Image of La Jolla Black's beach in the background looking North with the X-band vertically polarized scanning radar deployed by UMass in the foreground. (b) Ohio State University video cameras in foreground and SIO pier in the background.

	SWFSC	**Black's**
Parameter	**Value**	**Value**
Peak power	25 kW	25kW
Pulse length	100 ns	100 ns
Rotation rate	246 °/s	144 °/s
Center frequency	9.41 GHz	9.41 GHz
Bandwidth	10 MHz	10 MHz
Pulse pairs	4	5
Coherent averages	5	6
Effective PRF	1.06 kHz	0.8 kHz
DAQ sampling rate	20 MHz	20 MHz
Range resolution	15 m	15 m
Operation interval	55 min/hr	55min/hr
Height	70 m	12 m

TABLE I
OPERATION PARAMETERS OF RADARS.

to pulse and it is therefore termed an incoherent source.

Doppler processing relies on the precise knowledge of the starting phase of the transmitted pulse. In a coherent system it is safe to assume that all the transmitted pulses have the same starting phase and Doppler processing techniques, described in section II can be used. This is not true for an incoherent system. In order to be able to apply the same techniques the starting phase of the transmitted signal needs to be recorded and then subtracted from the incoming echo before further Doppler processing is done.

During NCEX the radar on the roof of the SWFSC building and the one situated at the parking lot of the Black's beach were operated using parameters summarized in Table I. The resulting range resolution of the radars was approximately 15 m while the azimuth resolution ranged from 2.2 m at the minimum range (140 m away from the radar site) to approximately 17 m at 1 km radial distance from the radar due to beam spreading.

2) Video camera hardware: The video cameras were installed and operated by Ohio State University. Two Sony DC10 2/3 inch analog video cameras were mounted on the NOAA SWFSC building next to the radar, shown in Figure 2(b). Video images were transmitted over an RF link to a receiving station at the end of the Scripps Pier approx. 1 km to the South, and digitized at 3 Hz using ATI TV-Wonder image capture boards in host PC's running Linux operating system. They were synchronized to GPS using a Horita master time code generator. Back-up analog images were recorded on time-lapse video tapes at 3.75 Hz. Video images were collected during daylight hours spanning dawn to dusk. Image to ground coordinate transformation as well as lens distortion corrections were done using the methods of [18].

C. Radar and video data processing

Data used in this paper were collected over nine minutes beginning 1000 PST on 31 October 2003. These data are of particular interest since both radars and cameras collected data at approximately the same time.

Radar data are naturally referenced by range and azimuth. Both video and radar data sets were converted into a common right-hand Cartesian coordinate system with positive y-axis pointing North and positive x-axis pointing East with the origin located near SIO pier piling number three.

The first step in georeferencing radar data is conversion of radar slant range to true ground range. Once the slant ranges have been translated to ground ranges, the pixel locations are translated and converted to Universal Time Mercator (UTM) northings and eastings. The radar location was surveyed by NRL and its exact position in terms of latitude and longitude is known. The final step in georeferencing routine converts the UTM pixel positions to OSU camera coordinate system.

During the experiment the position of the radar spinner was not calibrated precisely with respect to the true North. Hence the rotation angle from the radar coordinate system to the OSU camera coordinate system is not precisely known. To refine this, we used the position of the directional buoy, imaged by the radar as a bright spot within the Scripps canyon. Radar images are rotated such that the buoy signature

in time-averaged radar image is aligned with the recorded GPS position. The rotation angle that minimizes the difference between the actual buoy location and the one obtained from the radar image is used for georeferencing [19].

The video data were smoothed onto one meter cross-shore resolution (x-direction) and a 20 m alongshore resolution (y-direction), while the radar data had an approximate 15 m radial range resolution (approximately alongshore) and continually decreasing resolution in the cross-shore direction due to beam spreading with increasing range distance. The location of the radar (and video cameras) on the roof of SWSFC building was such that the radial velocity is very nearly alongshore at NCEX.

Figure 1(a) represents a 9 min average of radar received power given by $P = 10\log\langle|E_i|^2\rangle$, where $\langle\rangle$ represents an average of i samples of received echo (E) magnitude and phase. The ground coverage of the overlapping video used in this study is shown in Figure 1(b). A 9 minute time averaged mosaic of the overlapping camera views is shown. The figures 1(a) and (b) are the result of the georeferencing and consequent conversion of both data sets to the OSU coordinate system. They confirm the validity of the georeferencing procedures as the bright features in the surf are collocated in both video and radar images.

The radar velocity estimates were obtained using equation (2) and PIV estimates were obtained using equation (5) given in section II. As the radar only measures the radial component of surface velocity from its location, the bi-directional PIV vector velocity estimates were projected into radar's radial direction using,

$$v_r = v_x \hat{r_x} + v_y \hat{r_y} \tag{6}$$

where v_x and v_y are PIV-derived cross- and alongshore components of surface video velocities, $\hat{r_x}$ and $\hat{r_y}$ are the unit vectors given by

$$\hat{r_x} = \frac{x - x_0}{\sqrt{(x-x_0)^2 + (y-y_0)^2}}$$
$$\hat{r_y} = \frac{y - y_0}{\sqrt{(x-x_0)^2 + (y-y_0)^2}} \tag{7}$$

where x, y are x and y coordinates of the PIV pixel and x_0, y_0 are coordinates of the radar site.

IV. Radar and PIV velocity comparison

A. Near alongshore velocity comparison

Figure 3 shows color contour images of 9 minute averaged SWSFC radar and PIV velocity over areas corresponding to the filed of view of the video cameras. The average was performed over 9 minutes starting at 1000 hrs PST on 31 October 2003. The velocity scale shown in Figure 3 ranges +/- 1.5 m/s and is colored the same in the radar and PIV surface velocity maps. The white region is outside video field of

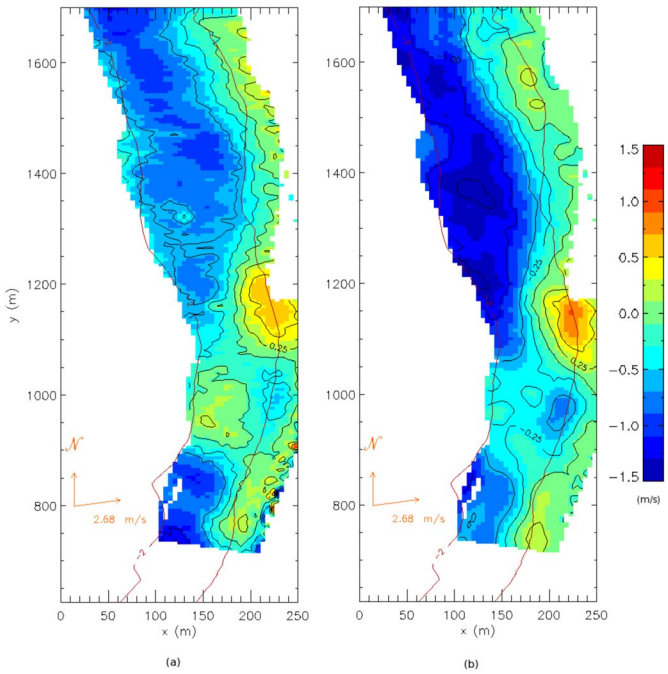

Fig. 3. Averaged radial surface velocity starting at 1000 hrs PST, October 31st 2003, along Black's beach, La Jolla, CA. (a) Image of 9 minute time averaged radar longshore velocity. (b) Image of 9 minute time averaged PIV longshore velocity over the surf zone.

view, on dry beach or represents missing data in both images. Bathymetry contours were plotted from averaged survey data collected by the Ohio State University. The hourly wind speed and direction as measured by the Coastal Data Information Program (CDIP) station at SIO pier [20] at 1000 hrs PST are shown in the bottom left hand corner of each image. Good agreement between radar and PIV is evident. Similarities of spatially varying longshore current features are clearly visible. At about 1100 m distance alongshore, the surface longshore current reverses direction with southerly flow near the shore (towards the radar; blue color) and northerly flow (away from the radar; red color). This feature is suggestive of a strong seaward flowing current and eddy-like structure at that location. In general, the radar and PIV surface velocity maps agree quite well over the 1 km alongshore region examined.

1) Spatial velocity comparison: Figure 4 shows the cross-shore transects where PIV velocity estimates were computed. These are overlaid on top of the 9 minute time averaged backscatter radar image. We find the extent of transects for which reasonable PIV estimates were obtained corresponds closely to the enhanced backscatter of the surf zone. This result is expected as the video contrast (hence signal strength) decays rapidly seaward of the surf, and is a useful check of the alignment of the two data sources. The transects shown were separated by 20 m in alongshore direction and are oriented shore-normal. In order to simplify spatial comparison both data sets were re-gridded to a 5 m by 5 m grid and hereafter we

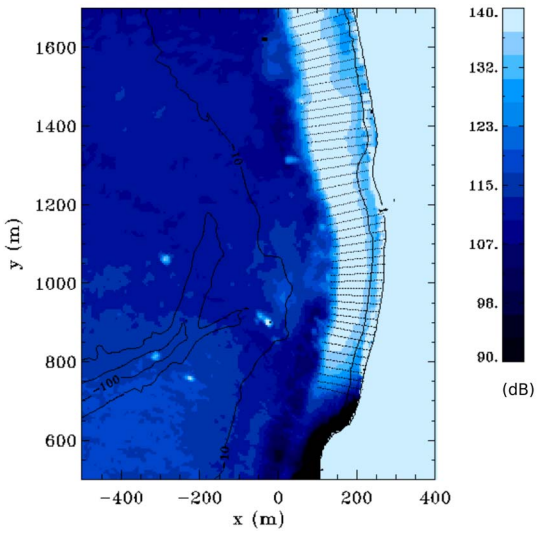

Fig. 4. Image of the average radar backscatter overlaid by video velocity transect locations (shore-normal lines spanning the bright region in the image) along the coast of Black's beach, La Jolla, CA.

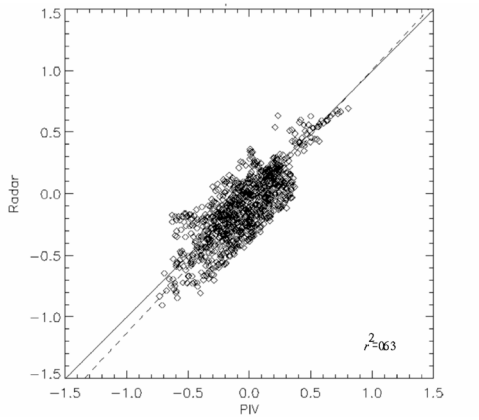

Fig. 5. Scatter plot of radar vs. PIV velocity estimates located strictly in the surf zone.

describe transects that are separated by 5 m in the alongshore direction and are positioned East-West, not shore-normal.

Figure 5 represents the scatter plot for data points extracted in the surf zone, eliminating the majority of points in the breaker and surf zone. The best fit line for these velocities, alone, has a slope of 1.02 very close to the ideal 1:1 slope fit even though scatter is still apparent. The rms difference in velocity values for the surf zone is 0.18 m/s while the correlation coefficient squared is 0.79. Thus, within the surf zone, the longshore velocities observed by both techniques are quantitatively consistent and with a small bias. Theoretically estimated radial component of the phase velocity in the surf zone was on the order of 2.0 m/s at the time of data collection. We do not see evidence of velocities of this order of magnitude in Doppler estimates. There is no evidence of velocity differences between Doppler and PIV velocities of this magnitude either. Investigating the spatial variation in

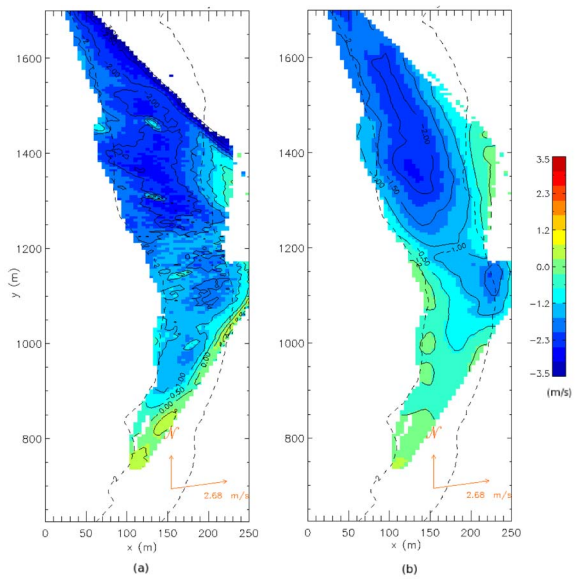

Fig. 6. Averaged radial surface velocity starting at 1000 hrs PST, October 31st 2003, across Black's beach, La Jolla, CA. (a) Image of 9 minute time averaged radar radial velocity. (b) Image of 9 minute time averaged PIV velocity over the surf zone.

longshore current profiles for several alongshore locations we noticed a trend. Velocity estimates over transects located closer to the radar and camera locations are observed to track each other closely in the surf zone while they differ in the swash and the breaker zone. However, the more distant transects show differences in velocity magnitudes both in the breaker zone and in the inner surf zone where the differences reach 0.6 m/s which is significantly higher than what can be attributed to either Bragg-resonant phase velocities or wind induced surface velocities (on the order of 0.2 m/s). In addition, at these distant ranges from the instrument locations, the PIV velocity estimates appear offset in azimuth from the radar near the mid-surf zone. This offset is likely due to the small uncertainty in video camera tilt angles in combination with the decreasing pixel resolution in the far-range.

B. Velocity comparison Black's beach radar

Figure 6 shows nine minute averages of the Black's beach radar and PIV radial velocities in the near cross-shore direction corresponding to the filed of view of the video cameras. The average was performed over 9 minutes starting at 1000 hrs PST on 31 October 2003. The velocity scale shown in Figure 6 ranges +/-3.5 m/s and is colored the same in the radar and PIV surface velocity maps. Just as in Figure 3 the white region is outside field of view of the cameras. While generating the 9 minute radar average we attempted to exclude bore velocities from the averaging process. This was achieved by excluding range bins whose backscattered power exceeded a threshold power assumed to correspond to the power of the bores. The PIV velocities were corrected for the bore velocity and smoothed prior to estimation of the radial component of the PIV velocity.

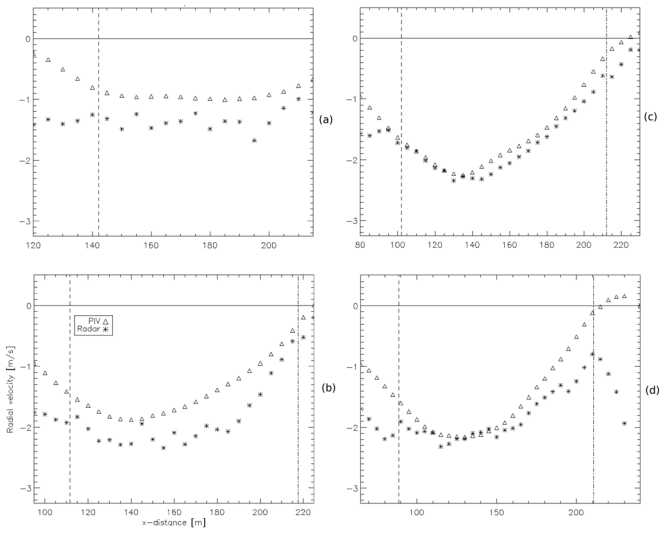

Fig. 7. Plots of cross-shore transects of radial component of surface velocity estimated by radar and video at (a) y=1200 m, (b) y=1300 m (c) y=1350 m, (d) y=1400 m. Dashed lines in each plot indicate inner edge of the breaker zone (left) and the outer edge of the swash zone (right).

The similarities of the two velocity maps are visible especially in the upper half of the image, where both techniques appear to estimate a strong negative flow.

1) Spatial comparison: To further investigate the similarities of the estimated velocity viewed from the Black's beach parking lot we look at cross-shore transects of velocity similar to the comparison of alongshore flows. The spatial variation of the estimated velocities is shown in Figure 7 for several cross-shore transects. The transects at 1200 m and 1300 m show greater discrepancy between radar and PIV velocities of up to 1 m/s. However the transects further along the shore, Figure 7(c) and (d) show smaller differences and the estimates track each other closely. The minimum velocity in the latter two plots is estimated at approximately -2.3 m/s by both radar and PIV while the maximum velocity tends to 0.0 m/s as we move closer to the shore (as x-coordinate increases). The cross-shore velocity profiles show greater discrepancies between radar and PIV velocities in the breaker and the swash zone while over the surf zone they track each other closely. As opposed to the alongshore comparison in this case the radar cross-shore resolution is constant while its alongshore resolution gets larger as we move toward breaker zone. This increase of radar's footprint might explain a larger velocity magnitude estimated by the radar.

V. Discussion

A possible explanation for the observed differences in alongshore velocities in the breaker zone is that radar and/or video derived velocities are influenced by steep breaking waves which at these locations are viewed obliquely, and these breaking wave phase velocities might add to the true mean surface velocities. The measured wavelength of ocean waves at the time of data collection was 6.74 m. According to Miche [21] the waves with the same wavelength and 0.9 m height or larger would break in 2 m water depth. The measured offshore wave height at the time was 1.31 m which would confirm the assumption of the presence of steep breaking waves in this area at the time the data set was collected. We consider next the environmental conditions that might produce such a bias.

At 1000 hrs PST the peak offshore rms wave height was 1.31 m with peak wave period 7.14 s and a peak wave direction of 282 degrees from the North, approximately 12 degrees from shore normal. The wave conditions were observed from a CDIP buoy located in 27 m water depth at 779 m alongshore and 233 m cross shore distance. Two other CDIP buoys located off Black's beach in 20 m and 100 m water depth showed similar conditions indicating a near-homogeneous incident wave field. Wave conditions in the surf were modified by wave-bottom interactions over the submarine canyons that produced alongshore variations in wave height and angle at the break point. This offshore refraction produces the complex surface flow observed over the study area. The peak direction indicates that the waves were not perpendicular to the radar and video look angles and so their apparent alongshore phase speed might contribute to measurements of surface velocity. Waves with 7.14 s peak wave period have deep water phase velocities of O(5-6 m/s) at the edge of the surf zone (in about 3 m water depth). The radial component of this velocity along the breaker zone is estimated at approximately -2.4 m/s. We do not see evidence of alongshore velocities of this magnitude either in the radar or PIV data. Frasier et al. [22] argue that the low-grazing X-band radar detects phase velocities of sea spikes that are significantly lower than the ones predicted in deep water. Assuming this can be applied to breaking waves in the shallow water the radial component of phase velocity of incident waves detected by radar would be on the order of -1.0 m/s. Since PIV velocity estimates in the breaker zone have a larger magnitude than radar this could suggest that video is more sensitive to influence of wave phase velocities of the breaking waves.

We found that near the breaker line, the rms velocity difference between radar and video alongshore surface velocity estimates is 0.33 m/s while in the surf zone this difference reduces by about half to 0.18 m/s. Also in this region PIV derived velocities are generally larger than estimates from radar. One source of discrepancy can be attributed to high uncertainties in PIV estimates that arise from contributions to the mean flow from wave propagation (direction and amplitude) and the initiation of wave breaking. Waves that propagate at a non-orthogonal angle of incidence have phase speed components in both the cross-shore and alongshore directions. When the waves initially break at an angle to the shoreline, the curling breaker along the crest of rapidly propagating waves is detected by the PIV technique. These higher velocities may increase the mean alongshore velocity estimate (as reported by [23]). As the waves on 31st October approach the shore from a northerly direction (driving the strong alongshore current to the South observed in the figures), we expect some contamination at the breaker line. Although

steps to eliminate the high velocities are made in the filtering procedures, it is likely that some bias in PIV estimates at the edge of the surf zone exists. This effect is less pronounced in the alongshore radar estimates.

Comparisons of radial velocities observed by the Black's beach radar and the PIV show that radar estimates are very sensitive to the phase velocity of waves and their orbital velocity when observed at almost orthogonal propagation to the look direction of the radar. A more careful removal of phase and orbital velocity is required to extract the true surface velocity.

In images of radar surface Doppler velocities, we note that the exposed beach and cliffs often return a non-zero Doppler velocity even though they are stationary targets. This is a consequence of the mechanical scanning of the antenna viewing a sloping surface where the centroid of scattering "moves" radially in the brief interval during which pulse-pairs are averaged. This effect is not present in the time-varying water surface which is on-average flat. Thus, the scatter in velocities seen by the radar at the shoreline may be due to this scanning effect.

In summary, at distances far from the radar and camera location, the differences between video and radar alongshore velocity estimates generally get larger. As range distance increases, both radar and video footprints become larger. Increase in footprint sizes leads to differences in spatial location between the two systems, that in regions of high spatial variation in the mean flow field would account for some of the observed differences in the far-range (greater than about 600 m from the camera). Small errors in image-to-ground transformation parameters lead to large spatial errors in pixel ground locations. Errors of 0.1 degrees in tilt angle result in 24.6 m ground errors at a range of 1000 m from the camera. As this region exhibits high spatial variability in mean flow patterns, spatial offsets in comparisons with radar can be large. This spatial error does not enter into radar estimates as distances to targets are precisely known from the time interval between transmitted and received pulses, given that there are no azimuth positional errors which is what was assumed in this analysis.

VI. Summary

Quantitative spatial velocity comparisons of alongshore velocity estimates show reasonable agreement between PIV and radar estimates for most of the surf zone, resulting in a best fit line with the slope of close to 1 and rms difference of 0.18 m/s. The spatial misregistration of data sets accounts for much of the scatter in the data and is believed to be responsible for the apparent space lag observed. On the other hand the spatial comparisons of near cross-shore velocities show greater discrepancies believed to be due to remnants of the bore and Bragg phase velocities found in the estimates.

Radar and video surface current measurement techniques have historically suffered from a lack of independent verification. As they both sense surface properties, it is often very difficult to compare remote observations to in-situ measurements that are necessarily obtained at depth (usually near the bottom well below the surface). The fact that both measurements indicate very similar surface velocities within the surf zone, and that both rely on very different mechanisms suggests that the true surface velocity is being captured with reasonable accuracy.

Acknowledgment

The authors gratefully acknowledge the able assistance of M. Okihiro and W. Pawlek of SIO (NCEX coordinator) in all logistical areas. G. Farquharson, Z. Tulu, M. Behn, and E. Knapp of UMass installed and operated the radar systems. J. Shore, G. Smith, J. Magalen, J. Long, and D. Welsh helped collect the video data. The video cameras mounted on the NOAA Fisheries building are part of Oregon State University's Argus program headed by R.A. Holman. This work was supported by the Office of Naval Research (Coastal Geosciences) under grants N00014-02-1-0239 to U. Massachusetts and N00014-02-1-0238 to Ohio State U.

References

[1] R. T. Guza and E. B. Thornton, "Observations of surf beat," *J. Geophy. Res*, vol. vol. 90, C4, pp. 3161–3172, 1985.

[2] W. E. Schmidt, B. T. Woodward, K. S. Millikan, R. T. Guza, B. Raubenheimer, and S. Elgar, "A gps-tracked surf zone drifter," *J. Atmos. Oceanic Tech.*, vol. vol. 20, (7), pp. 1069–1075, 2003.

[3] W. J. Plant, "The modulation transfer function: concept and applications," *Radar Scattering from Modulated Wind Waves, edited by G. J. Komen and W. A. Oost*, pp. 155–172, 1989.

[4] ——, "Microwave sea return at moderate to high incidence angles," *Waves in Random Media*, vol. 13, pp. 339–354, July 2003.

[5] G. Farquharson, S. J.Frasier, B. Raubenheimer, and S. Elgar, "Microwave radar cross sections and doppler velocities measured in the surf zone," *Journal of Geophysical Research*, vol. 110, C12024, 2005.

[6] K. S. Miller and M. M. Rochwarger, "A covariance approach to spectral moment estimation," *IEEE Transactions on Information Theory*, vol. 18 no.5, pp. 588–596, 1972.

[7] D. B. Trizna, "A model for doppler peak spectral shift for low grazing angle sea scatter," *IEEE Journal of Oceanic Engineering*, vol. OE-10 no. 4, pp. 368–374, 1985.

[8] D. Moller, S. J. Frasier, D. L. Porter, and R. E. McIntosh, "Radar-derived interferometric surface currents and their relationship to subsurface current structure," *Journal of Geophysical Research*, vol. 103, pp. 12,839–12,852, 1998.

[9] T. Lippmann and R. A. Holman, "Quantification of sand bar morphology: A video technique based on wave dissipation," *Journal of Geophysical Research*, vol. 94(C1), pp. 995–1011, 1989.

[10] S. G. J. Aarninkhof and B. Ruessnik, "Video observations and model predictions of depth-induced wave dissipation," *IEEE Trans. Geosci. remote Sens.*, vol. 42, pp. 2,612–2622, 2004.

[11] M. Raffel, C. E. Willert, and J. Kompenhans, *Particle Image Velocimetry: A practical primer*. Springer Verlag, 1998.

[12] R. J. Adrian, "Twenty years of particle image velocimetry," *Experiments in Fluids*, vol. vol. 39, (2), pp. 159–169, 2005.

[13] K. Holland, J. Puleo, and T. Kooney, "Quantification of swash flows using video-based particle image velocimetry," *Coastal Engineering*, vol. 44, pp. 65–77, 2001.

[14] N. G. Plant, K. T. Holland, and J. A. Puleo, "Analysis of the scale of errors in nearshore bathymetric data," *Marine Geology*, vol. vol. 191, (1), pp. 71–86, 2002.

[15] *The NCEX experiment, La Jolla, CA*, Woods Hole Oceanographic Institution, http://science.whoi.edu/users/elgar/NCEX/ncex.html.

[16] G. Farquharson, M. Behn, D. Perkovic, Z. Culcuoglu, and S. J. Frasier, "Microwave radar remote sensing of surface currents in the nearshore region," *Proc. IGARSS, Anchorage, AK*, vol. 2, pp. 1160–1163, 2004.

[17] L. Wetzel, *"On microwave scattering by breaking waves", in Wave Dynamics and Radio Probing of the Sea Surface*. New York: Plenum, 1986.

[18] K. T. Holland, R. A. Holman, T. C. Lippmann, J. Stanley, and N. Plant, "Practical use of video imagery in nearshore oceanographic field studies," *IEEE Journal of Oceanic Engineering*, vol. 22(1), pp. 81–92, 1997.
[19] G. Farquharson, "Microwave radar observations of nearshore ocean dynamics," Ph.D. dissertation, University of Massachusetts Amherst, 2005.
[20] *CDIP historic data*, UCSD, http://cdip.ucsd.edu/.
[21] R. Miche, "Undulatory movements of the sea in constant and decreasing depth," *Annales des Ponts et Chaussees*, pp. 25–78, 131–164, 270–292, 369–406, May-June, July-August 1944.
[22] S. J. Frasier, Y. Liu, and R. E. McIntosh, "Space-time properties of radar sea spikes and their relation to wind and wave conditions," *J. Geophys. Res.*, vol. no. 103, C9, pp. 18,745–18,757, 1998.
[23] J. A. Puleo, G. Farquharson, S. J. Frasier, and K. T. Holland, "Comparison of optical and radar measurements of surf and swash zone velocity fields," *J. of Geophys. Res.*, vol. vol. 108, no.C3, p. doi:10.1029/2002JC001483, 2003.